1994

Modeling and Experimental Validation of Area Constrained Ice Storage Systems

K. H. Drees
Johnson Controls

J. E. Braun
Purdue University

MODELING AND EXPERIMENTAL VALIDATION OF AREA CONSTRAINED ICE STORAGE SYSTEMS

K.H. Drees, P.E.
Johnson Controls, Inc.

J.E. Braun, Ph. D., P.E.
Purdue University

ABSTRACT

This paper describes the development and validation of an improved mechanistic model for predicting the thermal performance of an area constrained ice storage system. Experimental data was obtained from a fully instrumented thermal storage test cell located within the Herrick Laboratories, Purdue University. Results for both charging and discharging cycles are presented for a variety of inlet brine temperatures and flow rates. The model predictions agree well with the experimental data. The storage tank heat transfer effectiveness was found to be highly coupled to the flow rate but insensitive to changes in the inlet brine temperature. Supercooling and recalescence were also observed during the charging cycle.

NOMENCLATURE

variable list

$A_{\sim}$ = node surface area, ft^2
$c_{p,\sim}$ = specific heat constant pressure, Btu/lb-°F
$c_{v,\sim}$ = specific heat constant volume, Btu/lb-°F
$D_{\sim}$ = diameter, ft
$h_{\sim}$ = exterior convection coefficient, Btu/hr-ft^2-°F
h_{in} = interior convection coefficient, Btu/hr-ft^2-°F
$k_{\sim}$ = thermal conductivity, Btu/hr-ft-°F
L = node length, ft
$m_{\sim}$ = mass, lb
$R_{\sim}$ = Thermal resistance, °F/Btu
R_{spiral} = average spiral radius, ft
Ra = Rayleigh Number
$T_{\sim}$ = temperature, °F
$U_{\sim}$ = internal energy, Btu
u_{sl} = latent heat of fusion, Btu/lb

subscripts, ~

b = brine
b,i = brine inlet
b,o = brine outlet
ice = ice formation
in = tube interior
i-w = ice water interface
s = storage
tube = tube exterior
t-w = tube water interface
w = water

INTRODUCTION

Ice storage systems provide an effective means of reducing peak daytime electrical consumption by shifting operation of the primary cooling equipment to the nighttime. During a charging cycle, a 25% ethylene glycol and water (brine) solution is pumped through a reciprocating or centrifugal chiller and delivered to the storage tanks at approximately 23°F (-5°C) to 26°F (-3.3°C). During the discharging period; the chillers, ice storage tanks, or a combination of both provide chilled brine to the building at a temperature between 38 and 45°F (3.3-7.2°C).

The model described in this paper will predict the performance of area constrained ice storage tanks. The tank used to validate the model consists of an insulated cylindrical enclosure surrounding roughly 15,000 lineal feet (4572 m) of 1/2 inch (1.3 cm) o.d. polyethylene tubing. This tubing is divided into approximately 65 parallel circuits. The tubes are secured to plastic spacers which provide roughly 1/2 inch (1.3 cm) clearance between adjacent circuits. Each individual circuit forms a spiral located within a horizontal plane. Adjacent circuits are connected in an alternating sequence between two separate supply and return manifolds. This counterflow arrangement promotes uniform ice growth throughout the storage tank. The remaining enclosure volume is filled with 830 gallons (3.14 m^3) of water. A brine solution is pumped through the inside of the tubes and ice is either formed or melted outside the tubes. The close tube spacing minimizes the ice thickness and its corresponding thermal resistance. Near the end of the cycle, the growing ice formations intersect causing a rapid loss in surface

area and consequently heat transfer rate. Hence, the designation "area constrained". This same loss in surface area occurs when growing cylindrical water formations intersect in the discharging mode.

A model based upon physical parameters is useful in the design, application, or analysis of ice storage tanks. Jekel (1993) used fundamental thermodynamic and heat transfer relationships to develop a mechanistic area constrained ice storage model. The average model error was approximately 11% when compared to the manufacturers data. For simulation purposes, Strand (1992) empirically fit manufacturers data to relate the tank heat transfer rate to the tank inlet temperature, flow rate, and state of charge. This model is not useful for design, requires 14 coefficients to be calculated from performance data, and should not be extrapolated since it includes higher order polynomials. Stovall (1991) tested the latent performance of area constrained ice storage tanks. These tests did not include the sensible heat transfer modes and the brine temperature measurement accuracy was only ± 0.5°F (0.28 °C) which adversely effected energy balance calculations .

Due to the marginal accuracy of the Jekel model and the inherent limitations of empirical models, a new model, based on Jekel's work, was developed. Two primary enhancements were made. Interior convection correlations appropriate for the spiral tube geometry were used, and a finite difference grid was applied over the axial dimension of the parallel tubes to compensate for a non-uniform conductance area product. Since the accuracy of Stovall's energy balances was less than desired, and data was needed for both sensible and latent modes, new experimental data was used to validate the improved model.

MODEL DEVELOPMENT

There are 3 distinct modes involved in either charging or discharging an area constrained ice storage tank. The "sensible charging mode" starts with a discharged tank and consists of heat being sensibly removed until the average tank bulk water temperature is reduced to 32°F (0°C). The "unconstrained latent charging mode" is identified by the growth of cylindrical ice formations on the tube exterior. This mode continues until the outside of the ice formations initially intersect. The "area constrained latent charging mode" starts just after the ice cylinders intersect and continues until the water located between the tubes is completely frozen. The discharge cycle modes are similar to those of the charging cycle. The "unconstrained latent discharge mode" starts with a frozen tank and is characterized by the growth of cylindrical water formations about the tube exterior. It ends when the water formations initially touch. The "area constrained latent discharging mode begins after the water formations intersect and continues until all of the remaining ice is melted. The "sensible discharge mode" consists of sensibly adding heat to the tank until the water temperature approaches the inlet brine temperature.

Heat transfer through the tank enclosure is assumed to be negligible since the tank is well insulated. The interior tank volume is divided into "N" equally sized control volumes, or nodes, distributed along the axial length of the parallel tubes. The energy balance given by equation 1 is used to evaluate the nodal change in internal energy for the water and ice formations.

$$\frac{dU_s}{dt} = \dot{m}_b c_{p,b}\left(T_{b,i} - T_{b,o}\right) \tag{1}$$

The advection term in equation 1 is also equal to the heat transfer rate expressed in equation 2.

$$\dot{m}_b c_{p,b}\left(T_{b,i} - T_{b,o}\right) = \left[\frac{1}{R_{int} + R_{ext}}\right] \times \left[\frac{\left(T_s - T_{b,o}\right) - \left(T_s - T_{b,i}\right)}{\ln\left(\left(T_s - T_{b,o}\right)/\left(T_s - T_{b,i}\right)\right)}\right] \tag{2}$$

The interior thermal resistance, R_{int}, represents the sum of the interior convection and tube conduction resistances as shown in equation 3.

$$R_{int} = \frac{1}{A_{in} h_{in}} + \frac{\ln\left(D_{tube}/D_{in}\right)}{2\pi k_{tube} L} \tag{3}$$

The equation used to obtain R_{int} does not depend on the mode. The exterior resistance, R_{ext}, represents the sum of the thermal resistances which are unique to a particular ice/water formation

geometry or mode. The mode dependent expressions for the change in internal energy and R_{ext} are given in Table 1.

Table 1

Mode	$\frac{dU_s}{dt}$	R_{ext}	Notes
Sensible Charging	$m_w c_{v,w} \frac{dT_w}{dt}$	$\frac{1}{A_{tube} h_{t-w}}$	Entire tank water volume treated as single lump.
Unconstrained latent Charging	$-u_{sl} \frac{dm_{ice}}{dt}$	$\frac{\ln(D_{ice}/D_{tube})}{2\pi k_{ice} L} + \frac{1}{A_{ice} h_{i-w}}$	Cylindrical ice formations.
Area Constrained Latent Charging	$-u_{sl} \frac{dm_{ice}}{dt}$	$\frac{\ln(D_{ice}/D_{tube})}{2\pi k_{ice} L \phi} + \frac{1}{A_{ice}(AR) h_{i-w}}$	ϕ and (AR) are corrections for non-cylindrical geometry. (See Jekel)
Unconstrained Latent Discharging	$-u_{sl} \frac{dm_{ice}}{dt} + c_{v,w} \frac{d(m_w \bar{T}_w)}{dt}$	$R_{w1} = \frac{\ln(D_{\bar{T}_w}/D_{tube})}{2\pi k_w L}$	- Refer to figure 1. -R_{w2} is a conduction resistance.
Area Constrained Latent Discharging	$-u_{sl} \frac{dm_{ice}}{dt} + c_{v,w} \frac{d(m_w \bar{T}_w)}{dt}$	R_{w1} held constant at last value from previous mode	-Refer to figure 1. -R_{w2} changes to convection resistance, corrected for non-cylindrical geometry
Sensible Discharge	$m_w c_{v,w} \frac{dT_w}{dt}$	$\frac{1}{A_{tube} h_{t-w}}$	Entire tank water volume treated as single lump.

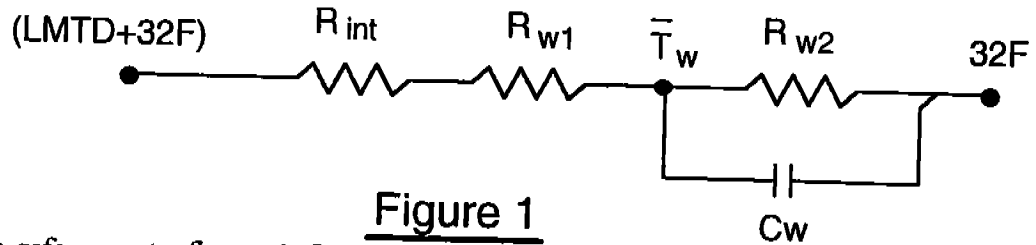

Figure 1

With reference to figure 1; R_{w1} is the water formation conduction resistance between the tube exterior and the water diameter corresponding to the location of the average water temperature, $\bar{T}_w$. For the unconstrained discharge mode, R_{w2} is the water conduction resistance between the location of $\bar{T}_w$ and the outside diameter of the cylindrical water formation. During the area constrained mode; the water formations intersect and flow paths are established, so natural convection correlations are used to obtain R_{w2}.

The non-steady energy balance, equation 1, is solved numerically by application of the explicit Euler method. The solution is marched forward in time using equal time steps. For each discrete time step, equations 1 and 2 are applied to each spatial node along the tube. The node heat transfer rate, change in internal energy, and outlet brine temperature are calculated. The outlet brine temperature is then used as the inlet temperature for the next node and the process is continued until the entire length of the tubing has been spanned. New nodal values for the ice or water mass are calculated from the internal energy changes. This updated information is used to determine new nodal thermal resistance values to be used in the next time step. The solution is marched forward in time until the storage tank is either fully charged or discharged.

External natural convection coefficients are obtained from equation 4 which applies to a long horizontal cylinder. The interior convection coefficient is calculated using relationships developed

$$Nu = \frac{h \cdot D}{k_w} = 0.48 \cdot Ra^{0.25} \tag{4}$$

specifically for spiral and helical tube geometries. The critical Reynolds number ($Re_{critical}$) associated with the change from laminar to turbulent flow is difficult to distinguish in a curved tube. Srinivasan (1970) recommends the following correlation to establish the critical Reynolds number.

$$Re_{critical} = 2100\left[1 + 12\left(\frac{2R_{spiral}}{D_{in}}\right)^{-0.5}\right] \tag{5}$$

For the ice storage system considered in this study, $Re_{critical}$ is approximately 5000. Over the practical range of operation, the Reynolds number does not exceed 5000 for this geometry. Kubair (1965) correlated the Nusselt number associated with fully developed laminar flow in a spiral tube according to equation 6.

$$Nu = \frac{h_{in}D_{in}}{k_b} = 8.14\left(1.98 + 1.8\frac{D_{in}}{2R_{spiral}}\right) \tag{6}$$

Nusselt numbers obtained for the spiral geometry are typically 2 to 5 times greater than those corresponding to the straight tube correlation that Jekel used. The spiral tube correlation was used to estimate the interior convection coefficient throughout this study.

Model Results

Heat exchanger effectiveness, ε, is defined as the ratio of the actual to the maximum possible heat transfer rate. Effectiveness is a useful performance index for presenting results since it is directly related to the thermal resistance and can be used to easily calculate heat transfer rates. For the area constrained tank geometry, ε reduces to a ratio of two temperature differences as shown in equation 7.

$$\varepsilon = \frac{\dot{q}_{actual}}{\dot{q}_{max}} = \frac{\dot{m}_b c_{p,b}(T_{b,i} - T_{b,o})}{\dot{m}_b c_{p,b}(T_{b,i} - T_s)} = \frac{(T_{b,i} - T_{b,o})}{(T_{b,i} - T_s)} \tag{7}$$

For the effectiveness results presented in this paper, the value of T_S is assumed to be 32°F (0°C) for all four latent modes. During the sensible discharge mode, T_S rises above 32°F (0°C). However, for consistency, the value of T_S used in equation 7 is assumed to be 32°F (0°C). For the sensible charging mode the actual tank temperature is used to avoid ε values greater than 1.

The effect of several variables on simulated tank performance is shown in figures 2 and 3 for charging and discharging. The tank is considered to be fully charged when all of the water located between the tubes is frozen. It is completely discharged when T_S approaches the inlet brine temperature. Over the first 3/4 of either cycle, ε drops slowly as the ice or water formations grow. The discharge effectiveness drops faster than the charging values since the thermal conductivity of water is approximately 3 times less than ice. During the last quarter of either cycle, ε drops quickly due to the

FIGURE 2
Chrg. Effectiveness = f (Tb,i, gpm, charge)

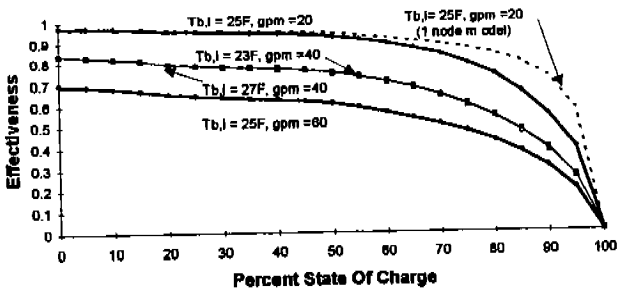

FIGURE 3
Dischrg. Effectiveness = f (Tb,i, gpm, chrg)

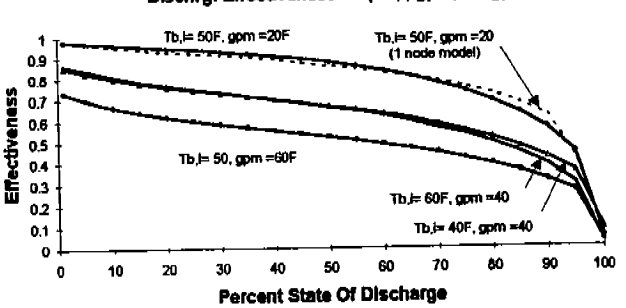

rapid loss in surface area. For both models, the effectiveness is shown to be strongly coupled to the flow rate and insensitive to the inlet brine temperature. This result was also observed for several other flow

rates and inlet temperatures which are not shown due to space limitations. For both models; improvements in the numerical solution, attributed to increasing the number of axial nodes, became insignificant after 3 nodes. It was also determined that a 2 minute time step provided good results. A separate trace (dashed) was included in both figures 2 and 3 to illustrate the worst case error attributed to using a single node model similar to that used by Jekel. The single node model provides relatively good accuracy during the unconstrained latent modes, but tends to over predict the effectiveness in the area constrained modes.

MODEL VALIDATION

A test cell was constructed to validate the ice storage model over a wide range of operating conditions. A chiller with a screw compressor is used to charge the storage tank. The tank is discharged by transferring heat into a hot water shell and tube heat exchanger. A direct digital control system, with 16 bit input resolution, was employed to perform the data acquisition and control functions. Temperature measurements were made with precision platinum RTDs installed in insertion wells lined with thermally conductive grease. All RTDs were two point calibrated at 32°F (0°C) and 70°F (21.1°C) to within 0.05°F (0.028°C). System and tank flow measurements were made with dual-frequency excitation magnetic flow meters (0.5% of reading accuracy) installed with a minimum of 25 unobstructed up and down stream pipe diameters. A schematic of the test cell is shown in figure 4.

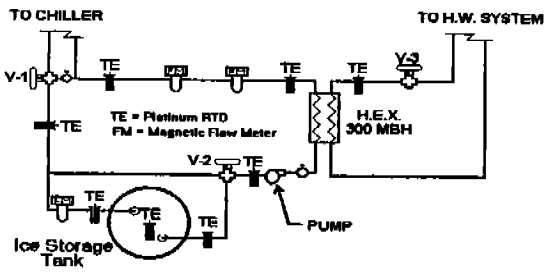

Figure 4, Test Cell Schematic

Test Results

Figure 5 compares the results predicted by the discharge model to data obtained from the test cell. In the legend, the model predictions are denoted by a leading "M" and the experimental data with a "D". The average deviation between the model and the data is 2.7% of the data point value, within the range of 0 to 75 percent state of discharge. This corresponds to all of the unconstrained and approximately 1/2 of the area constrained latent discharging modes. After approximately 75 percent state of discharge, the data does not correlate well with the model. This occurs since several geometrical coefficients must be extrapolated forward in time after the water formations initially intersect. During the beginning of the area constrained mode; these extrapolated values work well, however in the last half of the mode, ice starts to break free of the tubes and the geometry becomes indeterminate. After the ice has melted, the

FIGURE 5
Discharge Data vs. Model Predictions

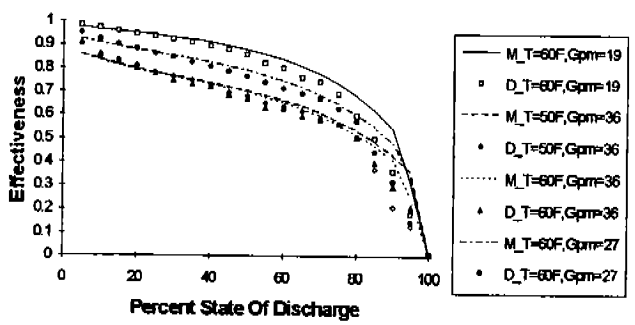

FIGURE 6
Charging Data vs. Model Predictions

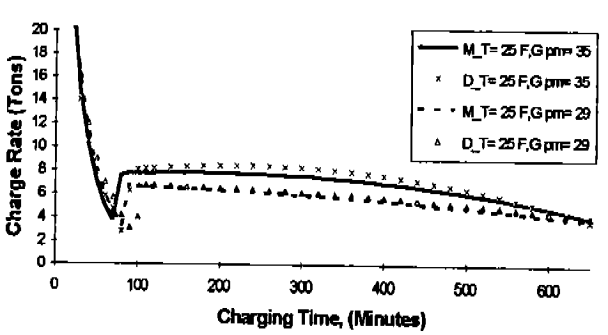

model again accurately predicts the tank performance, namely a linear relationship between state of discharge and effectiveness.

Figure 6 compares the charging model predictions with the test data. In this plot, the heat transfer rate is shown as a function of flow rate and state of charge, instead of effectiveness. On average, the model predictions are 6.3% below the values of the measured data. The portion of the curves preceding the discontinuity correspond to the sensible charging mode. The remainder of the curves include the entire unconstrained and the first half of the area constrained charging modes. During the last half of the area constrained mode, which is not shown in figure 6, the model over predicts the heat transfer rate because a reduction in the LMTD caused by ice formation supercooling is not considered.

The discontinuity which occurs in the range of 70-90 minutes is the result of recalescence occurring within the tank. Simply stated, recalescence is a flash freezing occurrence associated with the thermodynamic instability of a supercooled liquid. For an initial tank temperature of 60°F (15.56°C), the supercooling begins at approximately 15% of capacity and continues until the discontinuity. The heat transfer rate then quickly rises due to the sudden increase in the tank temperature associated with the latent heat released from the rapidly formed ice. For this tank, approximately 250 lbs (113.4 kg) of ice forms within a 120 second time interval, raising the water temperature from 27°F (-2.8°C) to the phase change temperature. This phenomenon has the potential to create system operation problems. Instructions provided with the tank advise stopping the chiller when the temperature difference between the tank inlet and outlet drops below 4-5°F (2.2-2.8°C). Test data showed that supercooling will cause the temperature differential to drop below these guidelines for a short time period. This could cause an automatic control system to shut down the chiller at only ≈20% of charged capacity. In addition the surge potential for a centrifugal chiller is significantly higher at the increased lift and decreased load conditions associated with the supercooling. These problems will not occur, however, if a small amount of ice is present at the start of the charging cycle. The ice provides an adequate number of nucleation sites to prevent the supercooling and subsequent recalescence.

CONCLUSIONS

The model presented in this paper can be used to accurately predict the thermal performance of an area constrained ice storage tank, except during the area constrained discharging mode where the ice geometry is indeterminate. The model errors are less than half of those given by other mechanistic models presented in the literature. The heat transfer effectiveness is strongly coupled to flow rate but insensitive to inlet temperature changes. Potential operational problems associated with supercooling and recalescence should be considered in the initial equipment selections and control design.

REFERENCES

CMC. 1991. *Levload Ice Bank Performance Manual.* Product Literature. Englewood, NJ: Calmac Manufacturing Corporation.

Jekel, T.B., J.W. Mitchell, and S.A. Klein. 1993. *Modeling of ice storage tanks.* ASHRAE *Transactions* 99(1).

Kubair, V., N.R. Kuloor. 1965. *Heat transfer to Newtonian fluids in spiral coils at constant tube wall temperature in laminar flow.* Indian Journal Of Technology, Volume 3, pp. 144-146.

Srinivasan, P.S., S.S. Nandapurkar, and F.A. Holland. 1970. *Friction factors for coils.* Inst. Chem. Eng. *Transactions,* Volume 48, pp. T156-T161.

Stovall, T.K.. 1991. *CALMAC Ice Storage Test Report,* ORNL/TM-11582, August. Oak Ridge, TN: Oak Ridge National Laboratory.

Strand, R.K.. 1992. *Indirect Ice Storage System Simulation.* M.S. thesis, University of Illinois, Urbana-Champaign.